

## Article

# Comparison of the Therapeutic Effects of Native and Anionic Nanofibrillar Cellulose Hydrogels for Full-Thickness Skin Wound Healing

Raili Koivuniemi <sup>1,2,\*</sup>, Qian Xu <sup>2,\*</sup>, Jasmi Snirvi <sup>1</sup>, Irene Lara-Sáez <sup>2</sup>, Arto Merivaara <sup>1</sup>, Kari Luukko <sup>3</sup>, Markus Nuopponen <sup>3</sup>, Wenxin Wang <sup>2</sup> and Marjo Yliperttula <sup>1</sup>

<sup>1</sup> Division of Pharmaceutical Biosciences, Drug Research Program, Faculty of Pharmacy, University of Helsinki, 00790 Helsinki, Finland; jasmi.snirvi@helsinki.fi (J.S.); arto.merivaara@helsinki.fi (A.M.); marjo.yliperttula@helsinki.fi (M.Y.)

<sup>2</sup> The Charles Institute of Dermatology, School of Medicine, University College Dublin, D04 V1W8 Dublin 4, Ireland; irene.lara-saez@ucd.ie (I.L.-S.); wenxin.wang@ucd.ie (W.W.)

<sup>3</sup> UPM-Kymmene Corporation, 00100 Helsinki, Finland; kari.luukko@upm.com (K.L.); markus.nuopponen@upm.com (M.N.)

\* Correspondence: raili.koivuniemi@helsinki.fi (R.K.); qian.xu@ucd.ie (Q.X.); Tel.: +358-445679201 (R.K.); +353-874678572 (Q.X.)

**Abstract:** Nanofibrillar cellulose (NFC)-derived dressings such as films, hydrogels, and aerogels are one of the favorable materials for wound healing due to their proper mechanical properties and water holding ability. However, the therapeutic differences between native and anionic NFC materials are rarely studied. In this report, we compared the differences and addressed the regenerative potential of native and anionic wood-derived NFC hydrogels for wound treatment. In vitro characteristics of the hydrogels were detected using scanning electron microscopy, rheological measurements, and swelling and hemolytic activity assays. Skin regeneration at an early stage after hydrogel treatment was analyzed using an in vivo splinted excisional full-thickness skin wound model in C57BL/6 mice. Both native NFC and anionic NFC (ANFC) hydrogel with differing mechanical and surface properties were shown to be biocompatible. Surprisingly, wounds treated with NFC and ANFC hydrogel did not show any statistical difference compared with control wounds and progressed through normal wound closure, inflammatory response, re-epithelialization, vascularization, and tissue maturation with no signs of fibrosis. The data show here for the first time the therapeutic performance of native and anionic NFC hydrogel in a wound mimicking human wound healing mechanisms. The mechanical properties of native and anionic NFC hydrogels such as the capability to modify material stiffness may also prove to be valuable in the management of wounds in the future.

**Keywords:** nanofibrillar cellulose; hydrogel; wound healing; splinted skin wound model



**Citation:** Koivuniemi, R.; Xu, Q.; Snirvi, J.; Lara-Sáez, I.; Merivaara, A.; Luukko, K.; Nuopponen, M.; Wang, W.; Yliperttula, M. Comparison of the Therapeutic Effects of Native and Anionic Nanofibrillar Cellulose Hydrogels for Full-Thickness Skin Wound Healing. *Micro* **2021**, *1*, 194–214. <https://doi.org/10.3390/micro1020015>

Academic Editor: Eiichi Tamiya

Received: 20 August 2021

Accepted: 30 September 2021

Published: 11 October 2021

**Publisher's Note:** MDPI stays neutral with regard to jurisdictional claims in published maps and institutional affiliations.



**Copyright:** © 2021 by the authors. Licensee MDPI, Basel, Switzerland. This article is an open access article distributed under the terms and conditions of the Creative Commons Attribution (CC BY) license (<https://creativecommons.org/licenses/by/4.0/>).

## 1. Introduction

Wound healing is a complex biological process, which occurs immediately at the time of injury and requires interactions between resident and migratory cell populations, soluble factors, and the extracellular matrix [1]. Clinically, wounds are categorized into acute and chronic wounds. The acute wounds are healed typically within days or a few weeks and they proceed through four overlapping and highly programmed wound healing phases: hemostasis, inflammation, proliferation (formation of granulation tissue), and remodeling [1,2]. If the wound is not healed within timely or orderly manner due to a failure at one or more phases of wound healing, it is characterized as a chronic wound.

To overcome problems related to disturbed wound healing, various tissue-engineering applications such as hydrogels, biologics, bioactive wound dressings, cell-based approaches, cultured epithelial autografts and biofabrication via 3D printing have been developed [3–8].

Among these, hydrogels are three-dimensional highly hydrated polymer structures resembling the natural structure of extracellular matrix (ECM) [9–11]. At the wound site, hydrogels are capable to absorb exudates, maintain moisture and offer a tissue-like structure [12]. Further, they can be loaded with different agents such as cells, growth factors, drugs, or antibacterial entities to stimulate wound healing [13]. Thus, they serve as a promising method to treat a wide variety of wounds, such as dry chronic wounds, pressure ulcers and burn wounds either as a temporary or a permanent dressing. Injection offers an appealing way for hydrogel delivery and most injectable hydrogels form “in situ” via chemical or physical crosslinking [13]. In addition, sprayable hydrogels can be delivered via simple application [14]. Recently, smart hydrogels have been developed, which respond to various external stimuli such as pH, temperature, or light [15].

A variety of synthetic and naturally derived hydrogels have been used for wound healing applications [12,13,16]. The common synthetic polymers used for hydrogel fabrication include polyethylene glycol (PEG), poly(vinyl alcohol) (PVA), poly(acrylic acid) (PAA), and polypeptides, which are attractive for tissue engineering purposes due to having controllable chemical and physical properties. Natural hydrogel polymers, on the other hand, provide excellent biocompatibility, biodegradability, and nontoxicity, and include, e.g., alginate, chitosan, collagen, carrageenan, hyaluronic acid, and silk fibroin. However, medical devices consisting of naturally derived hydrogels incorporate mostly animal origin materials even if they introduce a risk of disease transmission. The regulatory requirements of U.S. Food and Drug Administration (FDA) for medical devices that incorporate materials of animal origin are demanding and could be alleviated by using non-human and non-animal-derived materials in devices [17].

Among other biopolymers, cellulose offers a potential source for a hydrogel to be used for wound treatment [18]. Cellulose is an abundant polymer present in plant cell wall or produced by certain bacteria consisting of repeating units of  $\beta$ -D-glucose units held by  $\beta$ -1,4-glycosidic linkages [18]. Nanofibrillar cellulose (NFC) derived from wood pulp has a nanoscale structure with tunable properties and high elastic modulus in hydrogel form that makes it a promising human and animal origin-free material for wound treatment [19]. The wound healing potential of NFC results mainly from its highly hydrophilic nature and ability to retain moisture, which creates a moist wound environment known to enhance wound healing [20,21]. Previously, we have indicated the suitability of native NFC based wound dressing in split-thickness skin graft donor site treatment of patients, where it promoted efficient wound healing and epithelialization [22,23]. In a study by Nuutila et al. [24], on the other hand, NFC hydrogels were shown to inhibit wound contraction. Surface structure of native NFC can be modified with 2,2,6,6-tetramethylpiperidine-1-oxyl (TEMPO) oxidation to obtain an anionic charged structure [25,26]. Both native and anionic NFC has shown to be biocompatible as well as non-toxic for cells, and to provide a suitable scaffold for cell culturing [19,27,28]. Further, anionic NFC is suitable for drug delivery applications [29]. The stiffness of NFC hydrogels is easy to modify and can be tailored according to the varying stiffness of different tissues, which is an important aspect to consider.

In this report, we aimed to evaluate the effects of native (chemically inert) and anionic (surface charged) NFC hydrogel on wound healing in vivo using a splinted excisional full-thickness skin wound model in mice, which replicates the human wound healing process that occurs via re-epithelialization and granulation tissue formation instead of wound contraction typical for mouse wounds [30,31]. We focused on analyzing the NFC hydrogel properties in vitro, and wound closure, inflammatory response, re-epithelialization, granulation tissue formation, and blood vessel density in vivo. In addition, the presence of myofibroblasts in the granulation tissue and the expression of transforming growth factor (TGF)- $\beta$ 1 and collagen I were evaluated concomitantly with the activation of underlying mitogen-activated protein kinase (MAPK) signaling pathways facilitating wound healing.

## 2. Materials and Methods

### 2.1. Nanofibrillar Cellulose

Sterile native 1.5 w/w% NFC hydrogel (lots 120714619h and 119663917g applied for in vitro and in vivo assays, respectively), and 5.5 w/w% anionic NFC (ANFC) hydrogel (lot 11944) diluted to 3.2 w/w% ANFC hydrogel (UPM Biomedicals, Helsinki, Finland) were produced as described previously [19,29]. NFC raw material was aseptically collected from bleached birch pulp and homogenized using an industrial fluidizer. Purified pulp fibers were diluted with sterilized, ultra-high-quality water and fibrillated. To form ANFC hydrogel, the cellulose kraft pulp was chemically modified via oxidation before fibrillation to yield a carboxylic acid content of 1.0 mmol/g, which was determined by conductometric titration according to the standard SCAN-CM 65:02. Before in vivo application, ANFC hydrogel was sterilized by autoclaving at 121 °C for 15 min. pH indicator paper sticks (Fisherbrand, Fisher Scientific, Vantaa, Finland) were used to measure the pH of NFC hydrogels.

### 2.2. Scanning Electron Microscopy (SEM)

For SEM analysis, native and anionic NFC hydrogels were freeze-dried. First, samples were frozen by dipping in liquid nitrogen, and subsequently transferred to a freeze dryer (ScanVac CoolSafe, Labogene, Allerød, Denmark). Freeze-drying was performed in a vacuum for 72 h and the pressure in the chamber was decreased to 0.036 mBar. The temperature of an external condenser was −110 °C. For imaging, the samples were cut with tweezers and coated with platinum with Quorum Q150TS, turbomolecular-pumped high resolution coater (Quorum Technologies, Laughton, UK) for the analysis of the hydrogel inner structure. The morphology of the freeze-dried hydrogels was imaged using 2.0–5.0 kV and 2.5–4.0 spot in high vacuum with a scanning electron microscope FEI Quanta 250 Field Emission Gun SEM (FEI Company, Hillsboro, OR, USA). Pore sizes were measured from SEM micrographs using Leica Application Suite X (LAS X Core 3.7.4) software (Leica Microsystems, Wetzlar, Germany).

### 2.3. Rheological Measurements

The rheological measurements for NFC hydrogels were performed at +25 °C using HAAKE Viscotester iQ Rheometer (Thermo Fisher Scientific, Karlsruhe, Germany) equipped with a Peltier system for temperature control. HAAKE RheoWin 4.0 software (Thermo Fisher Scientific) was used to analyze the results. In all measurements, parallel steel plate-and-plate configuration was used (plate diameter of 35 mm, gap of 1 mm). Before the measurement, hydrogels were taken to room temperature for 30 min and allowed to rest for additional 2 min at the measurement plate with surface area of 962 mm<sup>2</sup>, at +25 °C in a volume of 0.96 mL. The linear viscoelastic region for the hydrogels was determined by controlled stress amplitude sweeps using constant angular frequency  $\omega = 1$  Hz and oscillatory stress between  $1 \times 10^{-4}$ –500 Pa. For frequency sweeps, the chosen oscillatory stresses were  $\tau = 5$  Pa and  $\tau = 30$  Pa for 1.5% NFC hydrogel and for 3.2% ANFC hydrogel, respectively. The angular frequency ranged from 0.6 to 125.7 rads<sup>−1</sup>. Triplicate samples were used for measurements.

### 2.4. Swelling and Water Retention Profile

To measure the swelling ratios of hydrogels, 1.5% native NFC hydrogel and 3.2% ANFC hydrogel were added as wet hydrogels into Transwell<sup>®</sup> permeable inserts (Merck, Darmstadt, Germany), and weighed before ( $W_0$ ) and after ( $W_t$ ) immersion in phosphate-buffered saline (PBS) on a 12-well plate. The plate was incubated at +37 °C at 150 rpm. At predetermined intervals ranging from 2 h to 21 days, the PBS buffer was removed and the swollen hydrogels on a transwell insert were blotted on a paper to remove the buffer on the surface and weighed. The swelling ratio was obtained from the following equation:

$$\text{Swelling ratio (\%)} = [(W_t - W_0)/W_0] \times 100\%, \quad (1)$$

The anticipated state of swelling equilibrium for the hydrogels was reached when no growth in swelling ratio was observed between two adjacent time points. The results were recorded and averaged from five replicate samples.

### 2.5. Hemolytic Activity

Human donor red blood cells (RBCs; Finnish Red Cross Blood Service, Helsinki, Finland) separated from the whole blood were washed three times with sterile PBS by centrifugation at 2000 rpm for 5 min. Subsequently, an RBC suspension was prepared by dispersing 200  $\mu$ L of RBC in 9.8 mL of PBS. Native 1.5% NFC hydrogel and 3.2% ANFC hydrogel (~20  $\mu$ L) were immersed into 1 mL of RBC suspension, and the mixture was incubated at +37 °C for 1 h. After incubation, the mixture was centrifuged at 2000 rpm for 5 min, and the supernatant collected for absorbance measurement at 540 nm using Varioskan LUX (Thermo Scientific, Waltham, MA, USA) microplate reader and SkanIt RE 6.0.2 software (Thermo Scientific). Triton X-100 (2%; Merck) and PBS were used as positive and negative controls, respectively.

### 2.6. Animals

C57BL/6 male mice were purchased from Charles River Laboratories (Portsmouth, UK) at the age of 7 weeks, and adaptively bred at least for 7 days before surgery. All animal experiments followed the EU Directive 2010/63/EU and were performed in compliance with the 3Rs and with the institute's policy on animal use and ethics. Animal experiments were approved by Animal Research Ethics Committee of University College Dublin (AREC-15-27-Wang), and by Health Products Regulatory Authority (AE18982/P091), Ireland. Animals were housed four animals per cage presurgery and two to four animals per cage postsurgery under standard conditions in a temperature-controlled room on a 12 h light/dark cycle at Biomedical Facility, University College Dublin. A standard laboratory diet was supplied ad libitum, and soft bedding material and a plastic tube shelter were provided for animals as an environmental enrichment. The animals were monitored and scored daily for behavior and appearance, for pain and discomfort, and for signs of infection before and after surgery until humanely euthanized, using the mouse grimace scale and a specific score sheet. In case of signs of increased pain, additional analgesia was provided for the animal, which was scored again after four hours. Power analysis for calculation of the animal number applied for the study is presented in the Supplementary Materials and Methods (Supplementary Table S1; Supplementary Figure S1). Animals were divided in different study groups using randomization (Supplementary Figure S2). Animals at 8–11 weeks of age were applied for surgery.

### 2.7. Surgical Procedure

Mice were anesthetized with isoflurane inhalation, and Buprenorphine (0.05 mg/kg) [32] was administered subcutaneously before surgery. The dorsal hair of the animals was shaved on either side of the spine, and the skin was disinfected with chlorhexidine, and sterilely draped. On the shaved dorsal surface, two full-thickness 6 mm-diameter circular excisional wounds were surgically created, one on either side of the spine. A sterile donut-shaped splint (outer diameter 14 mm, inner diameter 10 mm) fabricated from a 1.6 mm thick silicone sheet (Grace Bio-Labs, Bend, OR, USA) was then sutured with eight sutures using 4-0 Ethilon nylon sutures (Ethicon US LLC, Somerville, NJ USA) onto the surface of the skin surrounding the excision. Sterile native 1.5 w/w% NFC hydrogel and sterile 3.2 w/w% ANFC hydrogel were applied topically from a sterile syringe to the wound area at a volume of 100  $\mu$ L. Control wounds were left untreated. All the wounds were covered with a transparent Tegaderm Film dressing (3 M Health Care, St Paul, MN, USA) that was sutured on the silicone splint. Subsequently, wounds were covered with a gauze sutured on the skin, owing to difficulty of keeping the dressings in place. Animals were observed until they fully recovered from anesthesia. After surgery, pain relief was provided for all animals via subcutaneous injection of Buprenorphine (0.05 mg/kg) twice daily for three days.

At days 3 or 7 after surgery, animals were anesthetized again with isoflurane inhalation for sample collection. Full-thickness skin specimens containing the entire wound and wound margins were surgically collected after removal of the splint and partial removal of the hydrogel, divided in two halves and stored in 10% formalin for histological analysis, or frozen in liquid nitrogen and stored at  $-80\text{ }^{\circ}\text{C}$  for preparation of a tissue protein lysate. Animals were subsequently euthanized with an intraperitoneal injection of Pentobarbital sodium (100 mg/kg).

#### 2.8. Measurement of Wound Closure Rate

Wound beds were digitally photographed on days 0, 3, and 7 post-surgery. Wound area in pixels at each time point was evaluated by measuring the wound diameter using ImageJ 1.50i software, and the wound size calculated using the following equation:

$$\text{Wound area (\%)} = [\text{wound area (day } n\text{)}/\text{original wound area (day 0)}] \times 100\%, \quad (2)$$

#### 2.9. Exclusion Criteria

Exclusion criteria during the study included wound infection, premature detachment of hydrogel, or splint failure, which could have biased the results, and exaggerated pain, itch, or discomfort in animals, followed by euthanasia. Splint failure was determined as partial or complete detachment of splint, or more than three sutures released.

#### 2.10. Histopathology and Immunohistochemistry

Wound tissue samples fixed in 10% formalin for 24 h were embedded in paraffin, cut into  $5\text{ }\mu\text{m}$  sections, and stained with hematoxylin and eosin (H&E) or Masson's trichrome. Inflammation in the wound area and in wound margins was analyzed from H&E-stained sections by a pathologist, and graded based on the abundance of inflammatory infiltrate in the wound area, and inflammatory changes in the wound margins (extent of the tissue affected and intensity of the reaction) with a numerical scale from 1 to 4; 1 representing mild (no inflammatory cell infiltration or tissue reaction); 2, moderate (minimal neutrophilic infiltration and cell debris); 3, marked (necrotic debris and infiltration of neutrophils and/or macrophages); and 4, severe inflammation (purulent infiltrate of neutrophils and/or macrophages and necrotic debris). Grade 4 inflammation was considered as a necrotic deep inflammation suggesting infection, and those samples ( $n = 1$ ) were removed from the final analyses due to exclusion criteria.

For immunostaining, tissue sections were deparaffinized in xylene, rehydrated, and washed in distilled water. Antigen retrieval was performed in citrate buffer, pH 6 at  $100\text{ }^{\circ}\text{C}$  for 15–20 min, followed by blocking of endogenous peroxidase activity in 3%  $\text{H}_2\text{O}_2$  for 10 min. Non-specific staining was blocked with 5% bovine serum albumin (BSA; Merck, Darmstadt, Germany) in Tris buffered saline with Tween 20 (Merck)(TBS-T), and endogenous biotin using Avidin/Biotin Blocking Kit (Vector Laboratories, Burlingame, CA, USA). Sections were incubated with anti-rabbit ACTA2/ $\alpha$ -smooth muscle actin ( $\alpha$ -SMA) antibody (1:30; LifeSpan Biosciences Inc, Seattle, WA, USA) or anti-mouse proliferating cell nuclear antigen (PCNA) antibody (1:500; Santa Cruz Biotechnology Inc., Dallas, TX, USA) at  $+4\text{ }^{\circ}\text{C}$  overnight, followed by biotinylated goat anti-rabbit or goat anti-mouse IgG secondary antibody (1:1000; Abcam, Cambridge, UK) for 1 h at room temperature (RT). Antibodies were detected using VECTASTAIN Elite ABC Reagent (Vector Laboratories), followed by 3,3'-diaminobenzidine (DAB) horseradish peroxidase (HRP) substrate treatment (Vector Laboratories). Subsequently, the sections were counterstained with hematoxylin, dehydrated, and cleared in xylene.

The sections were scanned using Panoramic 250 Flash III brightfield digital slide scanner (3DHISTECH Ltd., Budapest, Hungary). The length of the newly formed epidermis and the thickness of the granulation tissue were measured from Masson's trichrome-stained sections using Panoramic Viewer 1.15.4 software (3DHISTECH Ltd.). ImageJ 1.50i software was used to evaluate  $\alpha$ -SMA staining intensity, the number of PCNA-positive

keratinocytes in a microscopic field by manual counting, and the deposition of collagen (blue intensity) from Masson's trichrome-stained samples.

### 2.11. Immunofluorescence

Deparaffinized and rehydrated sections were blocked using 5% BSA in phosphate-buffered saline (PBS)/Tween 20, followed by primary antibody incubation at +4 °C overnight with anti-rabbit CD31/platelet endothelial cell adhesion molecule (PECAM-1) antibody (1:500; Novus Biologicals, Abingdon, UK). Alexa Fluor 594 donkey anti-rabbit IgG (1:500; Thermo Scientific) was applied as a secondary antibody, and incubated for 1 h at RT. Slides were mounted with ProLong Diamond Antifade Mountant with DAPI (Thermo Fisher Scientific), imaged with Aurox Clarity Laser Free Confocal HS (Aurox, Oxford, UK) wide-field microscopy, and analyzed by counting manually the number of CD31-positive blood vessels with a visible lumen per microscopic field using Fiji ImageJ 1.51 software.

### 2.12. Western Blotting

Skin tissue samples were homogenized in Pierce RIPA lysis buffer (Thermo Scientific, ) supplemented with protease inhibitor and phosphatase inhibitor (Roche, Basel, Switzerland) using TissueRuptor (Qiagen, Hilden, Germany), and centrifuged at  $10,000 \times g$  at +4 °C for 20 min. Protein concentrations were measured using the Pierce BCA Protein Assay Kit (Thermo Scientific). Equal amounts of protein (40 µg) were separated by 10% or 12% SDS-PAGE and transferred onto a nitrocellulose membrane using Trans-Blot Turbo Transfer System (BioRad, Hercules, CA, USA). The membranes were then incubated with 5% BSA or non-fat milk in TBS-T for 1 h at RT, followed by incubation at +4 °C overnight with primary antibodies anti-rabbit ACTA2/ $\alpha$ -SMA (1:1000), anti-rabbit TGF $\beta$  (1:200; Cell Signaling Technology, Danvers, MA, USA), anti-rabbit Collagen 1/COL1A1 (1:1000; Boster Biological Technology, Pleasanton, CA, USA), anti-mouse ERK  $\frac{1}{2}$  (1:100) or anti-mouse p-ERK  $\frac{1}{2}$  (1:200) (Santa Cruz Biotechnology, Inc.), anti-rabbit p38 MAPK (1:500) or anti-rabbit Phospho-p38 MAPK (1:500) (Cell Signaling Technology), and anti-rabbit  $\beta$ -Actin (1:300; Bio-Rad). Peroxidase conjugated goat anti-rabbit IgG (1:50; Thermo Scientific) or goat anti-mouse IgG (1:500; Life Technologies, Carlsbad, CA, USA) secondary antibody was then applied on membranes for 1 h at RT and immunoblots were detected with Pierce ECL Western Blotting Substrate (Thermo Scientific). Relative amount of proteins were quantified using ImageJ 1.50i software.

### 2.13. Statistical Analysis

Data are expressed as mean  $\pm$  standard deviation (SD). Statistical significance between the groups was determined using one-way analysis of variance (ANOVA) followed by Tukey's honestly significance difference test. The significance level was defined as  $p < 0.05$ .

## 3. Results

### 3.1. Characterization of NFC Hydrogels

We evaluated the structure and porosity of NFC hydrogels using SEM. Both native NFC (nNFC) and ANFC hydrogel exhibited highly porous internal structures with average pore size of 13.2 µm for nNFC (range 3–29 µm) and of 30.6 µm for ANFC (range 12–59 µm) (Figure 1A). Thus, with the increase in the fiber content, the pore size increased. We then measured the pH of NFC hydrogels. Both native NFC hydrogel and ANFC hydrogel showed pH 7. This is because NFC is a sugar, of which alcohol groups show pH values of approximately 9 until it is neutral. ANFC hydrogel, on the other hand, is a Na<sup>+</sup> salt, which has about 20% of the hydroxyl groups ionized. However, because the wound environment is extremely buffered, and OH groups are weak acids, the pH of NFC hydrogels is always kept at the physiological level.

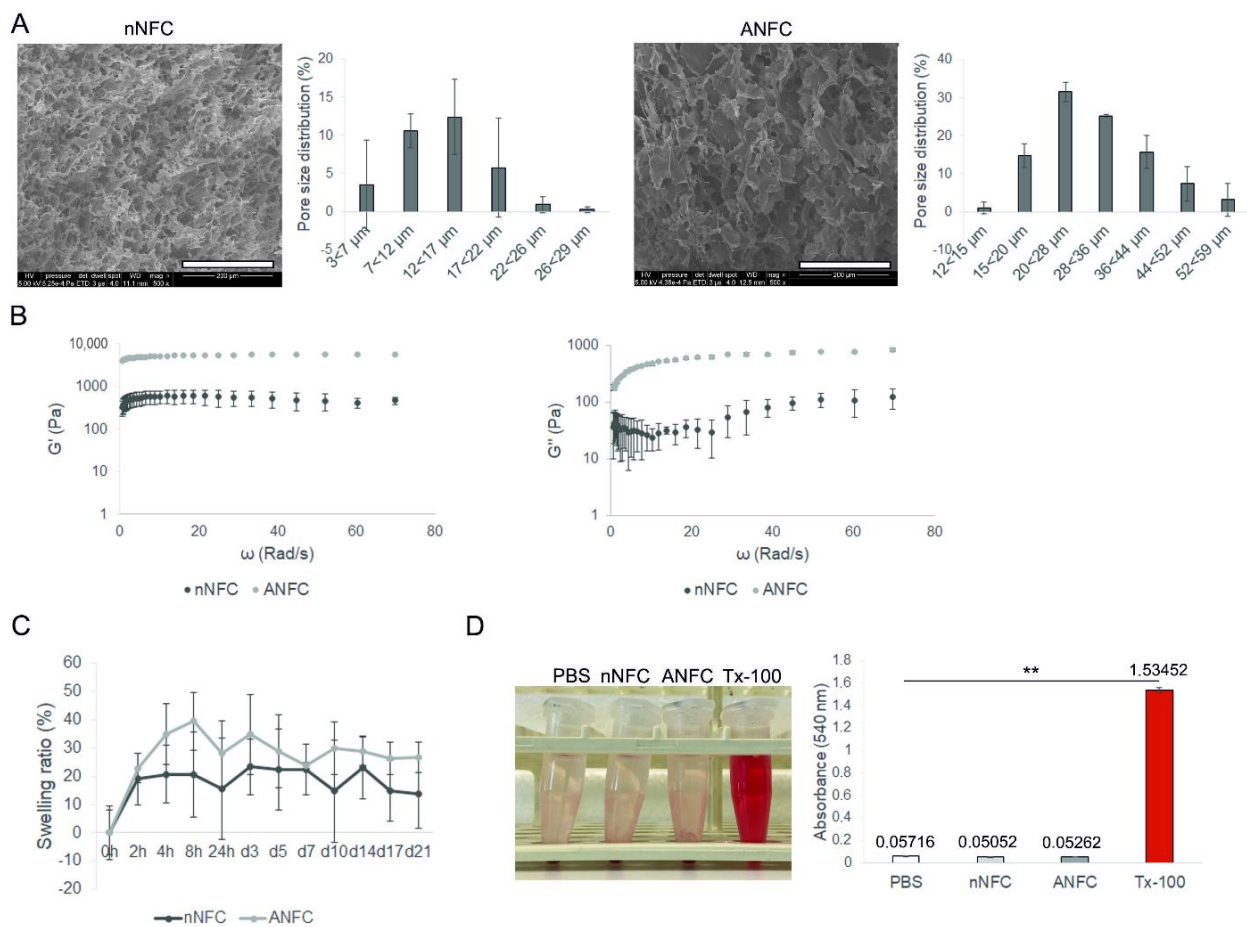


**Figure 1.** Properties of nanofibrillar cellulose (NFC) hydrogels. **(A)** Structural analysis and pore size distribution by scanning electron microscopy. The values are the mean  $\pm$  standard deviation (SD) ( $n = 2-3$ ). Scale bars, 200  $\mu\text{m}$ . **(B)** Storage ( $G'$ ) and loss modulus ( $G''$ ) of NFC hydrogels (mean  $\pm$  SD,  $n = 3$ ). **(C)** Swelling ratio of NFC hydrogels in phosphate buffered saline (PBS) at  $+37^\circ\text{C}$  up to 21 days (mean  $\pm$  SD,  $n = 5$ ). **(D)** Hemolytic activity of NFC hydrogels (mean  $\pm$  SD,  $n = 5$ ). PBS and 2% Triton X-100 (Tx-100) were used as the negative and positive control, respectively. \*\*  $p < 0.01$  Tx-100 vs. PBS, native NFC (nNFC) and ANFC. ANFC, anionic NFC; nNFC, native NFC.

The analysis of the viscoelastic properties of NFC hydrogels revealed higher storage ( $G'$ ) and loss modulus ( $G''$ ) in ANFC compared with native NFC (Figure 1B). In addition, storage modulus ( $G'$ ) values of both nNFC and ANFC were higher compared with loss modulus ( $G''$ ) values. The swelling behavior of NFC hydrogels was tested in PBS at  $+37^\circ\text{C}$  (Figure 1C). Native NFC hydrogel reached the equilibrium state of swelling within 2 h and ANFC hydrogel within 8 h. However, both NFC hydrogels remained stable in PBS for 21 days at  $+37^\circ\text{C}$  with agitation at 150 rpm without using preservatives, and no degradation was observed during the time period. The swelling ratios at equilibrium were approximately 20% for nNFC and 40% for ANFC. Since the hydrogels are highly porous, they contain two types of water, the water hydrating the polymer chains, and bulk water filling the pores. We further evaluated the biocompatibility of NFC hydrogels in vitro using hemolysis assay (Figure 1D). The results show that both nNFC and ANFC induce even less lysis of red blood cells than the negative control (PBS), suggesting that NFC hydrogels do not trigger hemolytic toxicity.

### 3.2. The Effect of Nanofibrillar Cellulose Hydrogels on Wound Closure and Inflammation

The effect of native and anionic NFC hydrogels on wound healing was evaluated in a splinted full-thickness excisional mouse wound model. Untreated wounds served as controls. Due to exclusion criteria, 36 wound samples (13 controls, 13 native NFC, 10 ANFC) harvested on days 3 or 7 post-surgery were available for analyses (Supplementary Table S2). None of the animals suffered from exaggerated pain, itch, or discomfort due to the treatments. Wound area was measured as indicated in Figure 2A. Representative photographs of the wounds at both time points are presented in Figure 2B. Compared with control wounds, wounds treated with native or anionic NFC did not promote wound closure on either of the time points (Figure 2C). At day 7, wound healing in control wounds was significantly progressed compared with day 3, while in wounds treated with native NFC or ANFC wound closure was not advanced (Figure 2C). These results suggest that NFC hydrogels do not affect wound closure.

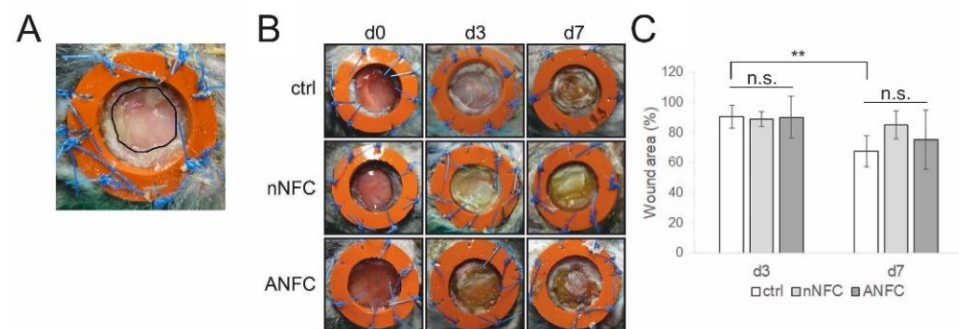


**Figure 2.** Wound closure is not affected by nanofibrillar cellulose (NFC) hydrogels in splinted mouse wounds. (A) A representative image of native NFC (nNFC)-treated wound on day 3 showing the wound area marked with a black circle applied to measure the wound diameter. (B) Photographs of wounds treated with native NFC (nNFC) or anionic NFC (ANFC) on the day of surgery (day 0; d0) and on days 3 and 7 after surgery. Control wounds were left untreated. (C) Quantitation of wound closure presented as the percentage of wound area on days 3 and 7 post-surgery. The values are the mean  $\pm$  standard deviation ( $n = 4-8$ ). \*\*  $p < 0.01$  d3 vs. d7. Ctrl, control; n.s., not significant.

At the beginning of inflammatory phase in wound healing, numerous leukocytes consisting mainly of neutrophils are infiltrated into the wound area during the first hours after the skin injury to clear the wound from invaded microbes and foreign material [1]. In our study, an independent pathologist analyzed the inflammatory changes from histological wound samples stained with hematoxylin and eosin on days 3 and 7 (Figure 3). On day 3, the dermis indicated various levels of inflammation. Dermal adipose tissue showed necrotic debris and hemorrhage, suggesting a marked trauma due to wounding, and moderate mixed inflammation. On day 7, a cellular crust consisting of abundant granulocyte debris and eosinophilic material covered the wound areas. The dermis exhibited mild to moderate inflammatory cell infiltration, and dermal adipose tissue showed mild to marked mixed inflammation. The inflammation in the wound area and in the wound margin were separately graded with numerical scales (Tables 1 and 2, respectively). No significant difference in acute inflammatory response was observed in native NFC- or ANFC-treated wounds compared with control, suggesting that wounds treated with NFC hydrogels progress through normal inflammation phase during wound healing. Further, there was no evidence of cell death due to the treatments.

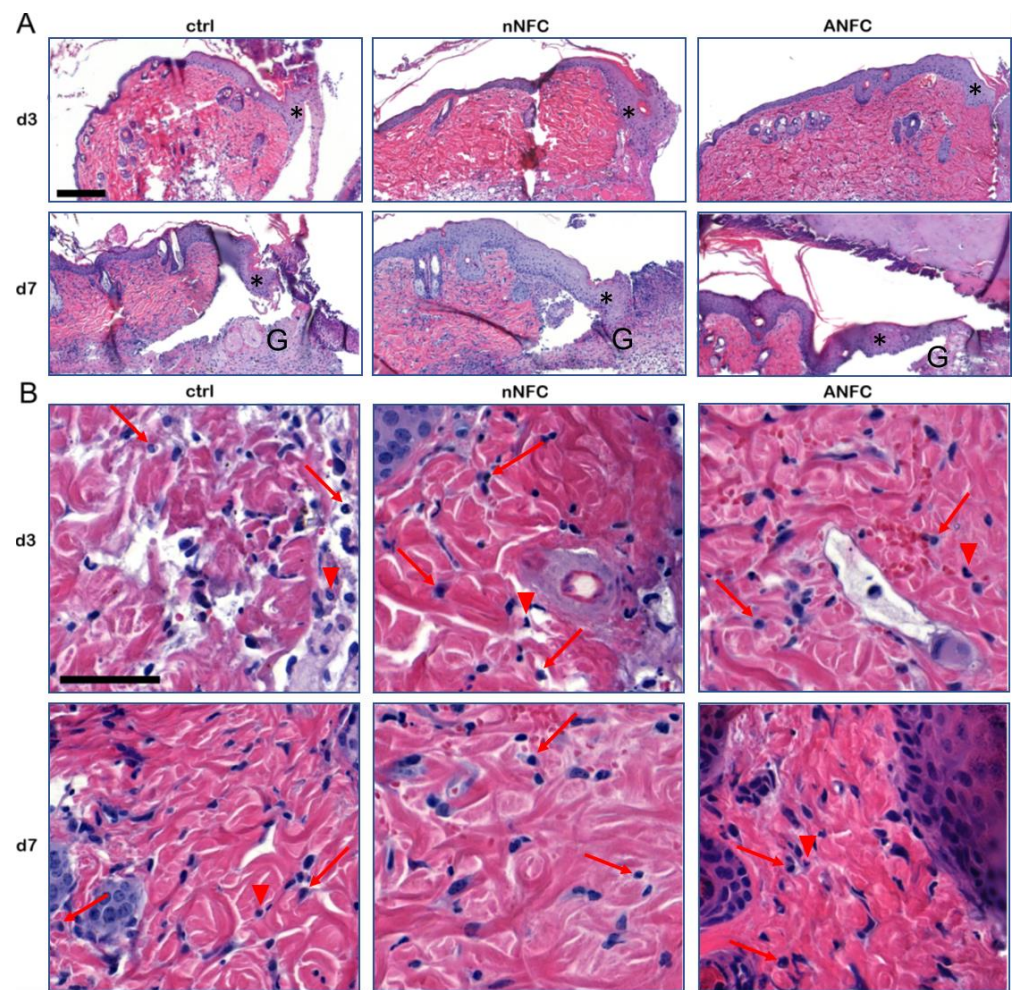


**Figure 3.** Representative hematoxylin and eosin staining images of wounds treated with native nanofibrillar cellulose (nNFC) and anionic NFC (ANFC), and untreated control. **(A)** On day 3, the epithelium at the wound margins exhibits mild to marked hyperplasia (asterisk). On day 7, the wound margin epidermis shows moderate to marked hyperplasia (asterisk). Some granulation tissue (G) is present. Scale bar, 200  $\mu$ m. **(B)** On day 3, the dermis shows moderate to no mixed inflammatory cell infiltration (mononuclear cells indicated with a red arrow and neutrophils with a red arrowhead) in control wounds, mild to no inflammatory cell infiltration in nNFC-treated wounds and mild mixed inflammation or no inflammatory cell infiltration in ANFC-treated wounds. On day 7, the dermis exhibits mild mononuclear inflammation (macrophages and lymphocytes) in control and mild to moderate mixed inflammation in hydrogel-treated wounds. Scale bar 50  $\mu$ m. Ctrl, control.

**Table 1.** Grading of inflammation in the wound area 3 and 7 days after wounding based on the abundance of inflammatory infiltrate.

Histopathologic Scale to Evaluate Inflammation							
Day	Group	Total	Grade 1	Grade 2	Grade 3	Grade 4	<i>p</i> Value
3	ctrl	5	0	2	3	0	0.129
	nNFC	4	0	1	3	0	
	ANFC	4	2	1	1	0	
7	ctrl	4	0	1	3	0	0.323
	nNFC	4	1	1	2	0	
	ANFC	3	2	0	1	0	

Numerical scales represent mild (1; no inflammatory cell infiltration); moderate (2; minimal neutrophilic infiltration); marked (3; infiltration of neutrophils and/or macrophages); or severe (4; purulent infiltrate of neutrophils and/or macrophages) inflammatory changes. Ctrl, control; ANFC, anionic nanofibrillar cellulose; nNFC, native NFC.

**Table 2.** Grading of inflammation in the wound margin 3 and 7 days after wounding based on the intensity of the inflammatory reaction and extent of the tissue affected as described in the materials and methods.

Histopathologic Scale to Evaluate Inflammation							
Day	Group	Total	Grade 1	Grade 2	Grade 3	Grade 4	<i>p</i> Value
3	ctrl	6	2	3	1	0	0.918
	nNFC	6	2	3	1	0	
	ANFC	6	2	2	2	0	
7	ctrl	4	0	0	4	0	0.6
	nNFC	5	0	1	4	0	
	ANFC	2	0	0	2	0	

Numerical scales represent mild (1; no tissue reaction); moderate (2; cell debris); marked (3; necrotic debris); or severe (4; purulent necrotic debris) inflammatory changes. Ctrl, control; ANFC, anionic nanofibrillar cellulose; nNFC, native NFC.

According to histopathologic evaluation, both native NFC and ANFC appeared biocompatible and induced no foreign body giant cell formation but showed infiltration of various cell types, mainly neutrophils in addition to few macrophages, into the hydrogels (Figures 3 and 4). Native NFC even exhibited some infiltration of mesenchymal cells and epidermal cells and was encapsulated by fibrous tissue in some samples (Figure 4B,C). These results point out an acute inflammatory response, which is characterized by neutrophil infiltration, but no pathological immune response towards the biomaterial involving development of foreign body giant cells (FBGCs) [33]. However, it cannot be ruled out that FBGCs are not forming at the later time points, which are not addressed in this study.

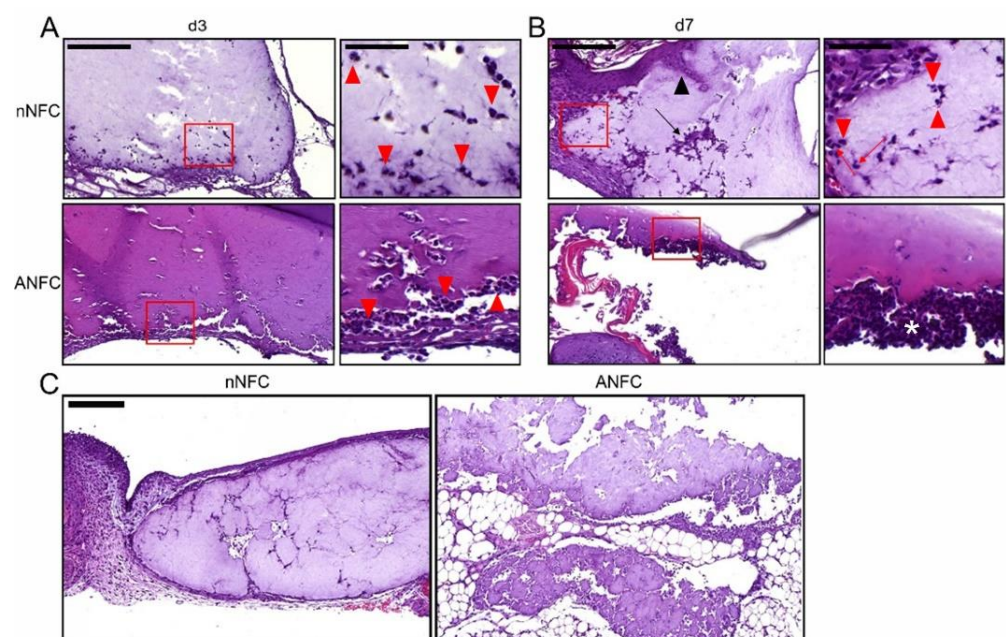


**Figure 4.** Cell infiltration into nanofibrillar cellulose (NFC) hydrogels. (A) Day 3. Native NFC (nNFC) hydrogel shows minimal, mostly neutrophilic infiltration, while there is minimal to moderate but largely superficial neutrophilic or mixed inflammatory infiltration into the anionic NFC (ANFC) hydrogel. Scale bar in the images on the left, 200  $\mu$ m. Higher magnification with neutrophils marked with red arrowheads is shown on the right, scale bar 50  $\mu$ m. (B) Day 7. Native NFC hydrogel is invaded mostly by neutrophils (red arrowhead) with few macrophages (red arrow), and small number of mesenchymal cells (black arrow) and epidermal cells (black arrowhead) infiltrating into the hydrogel in some samples. ANFC hydrogel shows minimal to marked infiltrates of neutrophil debris (asterisk).

Scale bar in the images on the left, 200  $\mu\text{m}$ . Higher magnification is shown on the right, scale bar 50  $\mu\text{m}$ . (C) On the left, native NFC hydrogel aggregate is enclosed in a layer of fibrin and a loose layer of cellular debris containing neutrophils, macrophages, and mesenchymal cells. On the right, fragmented ANFC hydrogel covers and submerges inside the adipose tissue. Scale bar, 200  $\mu\text{m}$ .

### 3.3. Nanofibrillar Cellulose Hydrogels Provide Efficient Wound Re-Epithelialization

Concomitantly with the inflammation phase, the wound healing continues with cell proliferation that facilitates the growth of a new epithelium and the granulation tissue. We observed hyperplasia to be present in the epithelium at the wound margin in all samples (Figure 3A). Further, we evaluated re-epithelialization in wounds from Masson's trichrome-stained wound sections by measuring the length of the neo-epithelium, i.e., the layer of keratinocytes growing into the wound area, as indicated by double-headed arrows in Figure 5A. Both native NFC and ANFC showed comparable re-epithelialization at day 3 and day 7 compared with control wounds (Figure 5A,B).

To analyze cell proliferation in the newly regenerated epidermis, the proliferating cell nuclear antigen (PCNA), a marker for proliferating cells, was detected in day 3 and 7 wound sections by immunohistochemistry to quantify the amount of positive keratinocytes (Figure 5C–F). NFC hydrogels showed similar levels of PCNA-positive keratinocytes in the epidermis compared with control (Figure 5D,F) indicating that cell proliferation in the epidermis was not significantly affected. Results presented herein propose that the growth of the new epidermal tissue progresses ordinarily in wounds treated with NFC hydrogels.

### 3.4. Granulation Tissue Formation Appears Normal in NFC Hydrogel-Treated Wounds

The growth of granulation tissue was evaluated from Masson's trichrome-stained sections by measuring its thickness. Wounds treated with NFC hydrogels showed equal granulation tissue compared with control (Figure 6A,B). The growth of granulation tissue is facilitated by dermal fibroblasts, which produce new ECM proteins such as collagen. The amount of collagen deposition was analyzed in the newly formed granulation tissue at day 7 from Masson's trichrome-stained sections that shows collagen fibers in blue. No significant difference in collagen deposition was observed after treatment with native NFC or ANFC compared with control (Figure 6C). These results suggest that NFC hydrogels provide normal granulation tissue development during wound healing.

### 3.5. Nanofibrillar Cellulose Hydrogels Provide Normal Angiogenesis and Tissue Maturation in a Wound

The expression of  $\alpha$ -SMA is considered as a marker of fibroblast differentiation into myofibroblasts that are essential for wound contraction and extracellular matrix (ECM) remodeling following tissue injury [34]. We therefore examined whether NFC hydrogels affect  $\alpha$ -SMA expression. The immunohistochemical staining at day 7 revealed similar expression levels of  $\alpha$ -SMA in wounds treated with NFC hydrogels compared with control wounds (Figure 7A,B). The  $\alpha$ -SMA expression levels were further confirmed by Western blot analysis of full-thickness wound samples, which showed similar results (Figure 7C). Considering that  $\alpha$ -SMA is also expressed in pericytes facilitating blood vessel maturation [35], and to study the effect of NFC hydrogels on wound vascularization, we addressed the level of angiogenesis in wounds by immunofluorescence staining of platelet endothelial cell adhesion molecule CD31 [36,37] (Figure 7D). Native NFC or ANFC did not affect the density of CD31-positive blood vessels compared with control (Figure 7E), suggesting that angiogenesis is not affected by NFC hydrogel treatment.

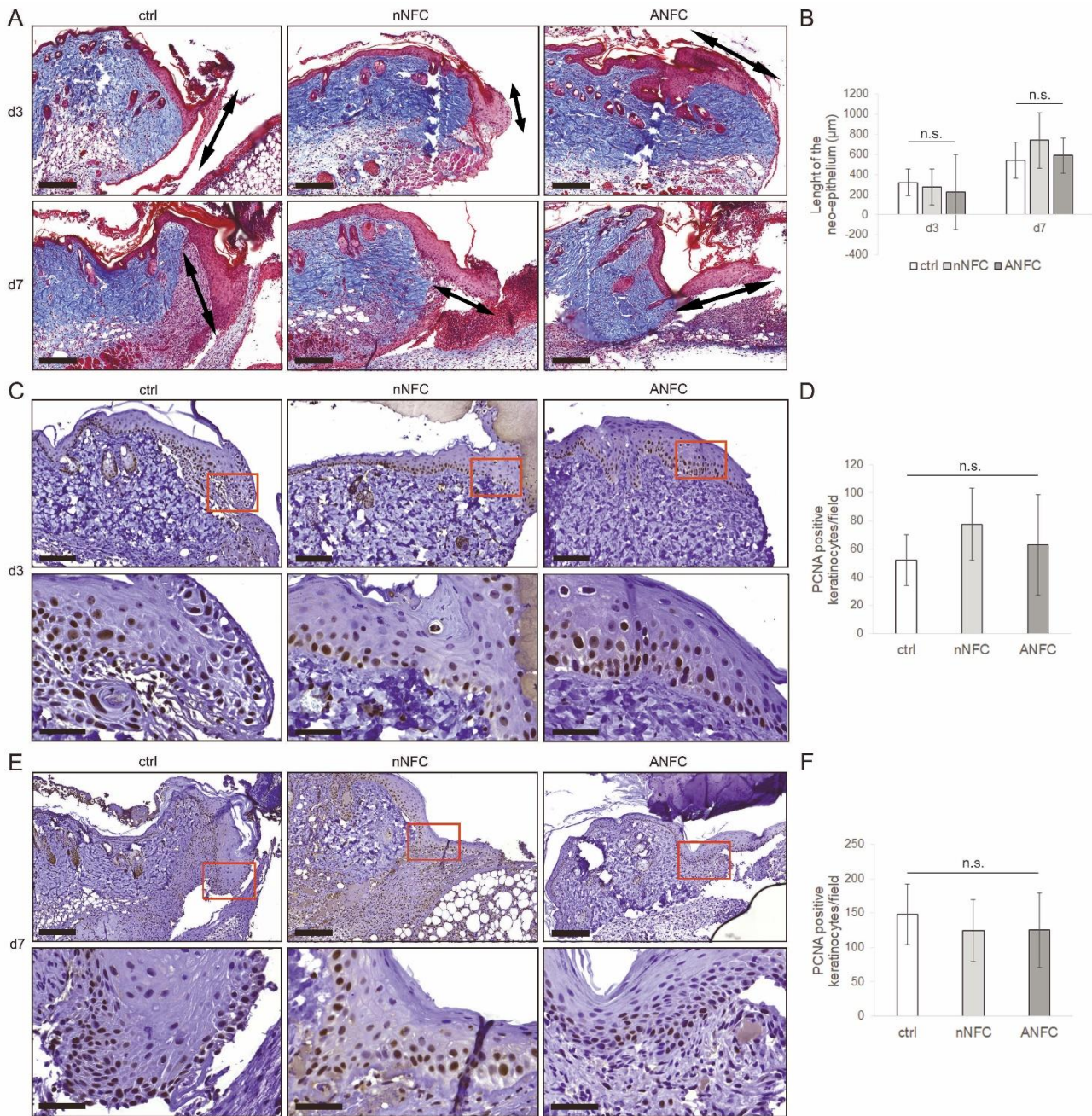


**Figure 5.** Re-epithelialization in control, native nanofibrillar cellulose (nNFC), and anionic NFC (ANFC)-treated wounds. (A) Representative images of Masson’s trichrome staining from the wound margin on days 3 and 7. The double-headed arrows indicate the length of the newly formed epithelium. Scale bars, 200 µm. (B) Quantitation of the length of the new epithelium from Masson’s trichrome-stained sections on day 3 and 7 showing normal re-epithelialization by NFC hydrogels. The values are the mean ± standard deviation (SD) ( $n = 4-7$ ). (C) Proliferating cell nuclear antigen (PCNA) staining of wound sections on day 3. Scale bars, 200 µm (top row), 50 µm (bottom row). (D) The number of PCNA-positive keratinocytes in the epidermis on day 3 is not affected by NFC hydrogels. The values present the mean ± SD ( $n = 6$ ). (E) PCNA staining on day 7. Scale bars, 200 µm (top row), 50 µm (bottom row). (F) The number of PCNA-positive keratinocytes on day 7 is comparable in wounds treated with NFC hydrogels compared with control (mean ± SD,  $n = 4-5$ ). Ctrl, control; n.s., not significant.

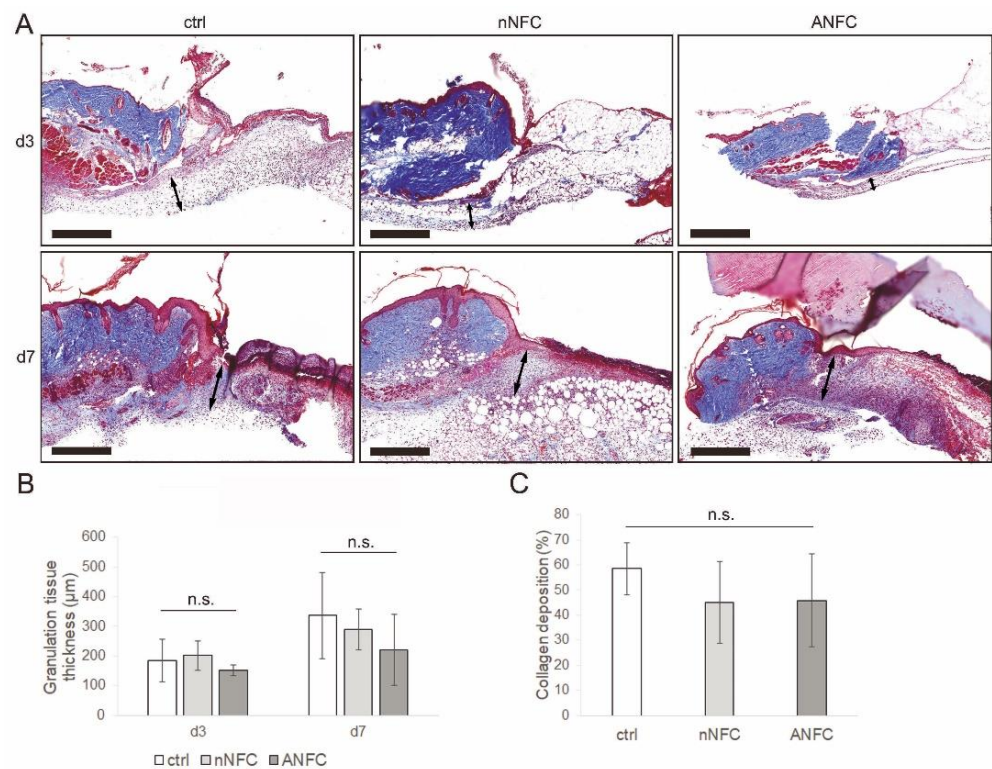


**Figure 6.** Granulation tissue formation in control, native nanofibrillar cellulose (nNFC)- and anionic NFC (ANFC)-treated wounds. **(A)** Representative images of Masson's trichrome staining from the wounds showing the granulation tissue on days 3 and 7. The double-headed arrows indicate the thickness of the granulation tissue. Scale bars, 500  $\mu\text{m}$ . **(B)** Quantitation of granulation tissue thickness on day 3 and 7 indicating equal growth of the granulation tissue in NFC hydrogel-treated wounds compared with control on day 7. The values present the mean  $\pm$  standard deviation (SD) ( $n = 4-6$ ). **(C)** NFC hydrogels do not affect the percentage of collagen deposition in the granulation tissue quantitated from day 7 Masson's trichrome-stained sections. The values are the mean  $\pm$  SD ( $n = 4-5$ ). Ctrl, control; n.s., not significant.

TGF- $\beta$ 1 is known to play various roles during the wound healing process. It is a pro-angiogenic factor that stimulates angiogenesis [38]. Moreover, TGF- $\beta$ 1 induces myofibroblast differentiation from fibroblasts, advancing fibrotic remodeling and tissue maturation via activation of  $\alpha$ -SMA [38,39]. However, its persistent activation is associated with fibrosis [40]. We therefore evaluated the expression of TGF- $\beta$ 1 in wounds by Western blotting to address whether NFC hydrogels increase fibrosis. The expression levels of TGF- $\beta$ 1 were comparable in NFC hydrogel-treated wounds and control wounds at day 7 (Figure 7F). The fibrotic remodeling was further examined by expression analysis of a fibrotic marker collagen I using Western blotting. The results show that the expression of collagen I is not affected by NFC hydrogels compared with control (Figure 7G). Overall, the results obtained herein confirm that NFC hydrogels do not induce fibrosis or significantly affect the collagen deposition.

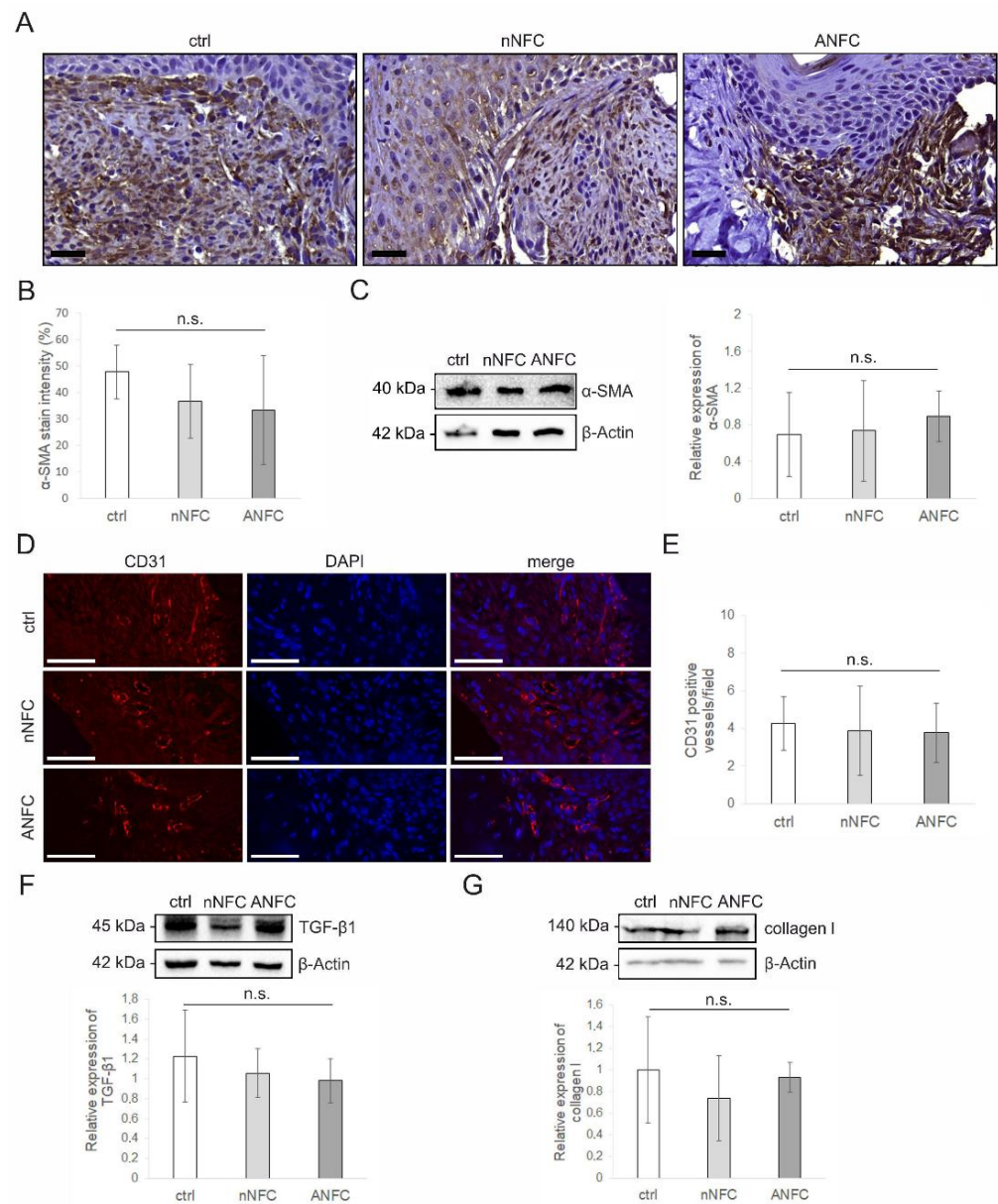


**Figure 7.** Granulation tissue remodeling and angiogenesis in control, native nanofibrillar cellulose (nNFC)- and anionic NFC (ANFC)-treated wounds. **(A)** Immunohistochemical (IHC) staining of wound sections with  $\alpha$ -smooth muscle actin (SMA) antibody on day 7. Scale bars, 50  $\mu$ m. **(B)** Quantitation from IHC staining showing no significant change in expression of  $\alpha$ -SMA in the granulation tissue by NFC hydrogels compared with control. The values present the mean  $\pm$  standard deviation (SD) ( $n = 4-5$ ). **(C)** Western blot showing expression of  $\alpha$ -SMA in control, and nNFC and ANFC hydrogel-treated wounds on day 7. Quantitation showing the mean  $\pm$  SD ( $n = 4-5$ ) is presented on the right. **(D)** Immunofluorescence staining of CD31 (red) and nuclei (DAPI; blue) in the granulation tissue on day 7. Scale bars, 50  $\mu$ m. **(E)** Quantitation of CD31-positive blood vessels from immunofluorescence staining showing no difference between NFC hydrogel-treated and control wounds. The values are the mean  $\pm$  SD ( $n = 4$ ). **(F,G)** Immunoblots and quantitations showing no significant change in the expression levels of TGF- $\beta$ 1 (**F**) and collagen I (**G**) in NFC hydrogel-treated wounds compared with control. The values are the mean  $\pm$  SD ( $n = 4-5$ ). Ctrl, control; n.s., not significant.

The phosphorylation of extracellular signal-regulated kinases (ERK) and p38 MAPK has been shown to improve wound healing by inducing the proliferation and migration of fibroblasts and keratinocytes [41–43]. Thus, we analyzed the phosphorylation state of ERK and p38 MAPK in wound samples by Western blotting. The results show that the phosphorylation of ERK and p38 MAPK in native NFC or ANFC hydrogel-treated wounds are comparable with control wounds (Figure 8A,B), suggesting further that tissue maturation during wound healing proceeds normally in NFC hydrogel-treated wounds.

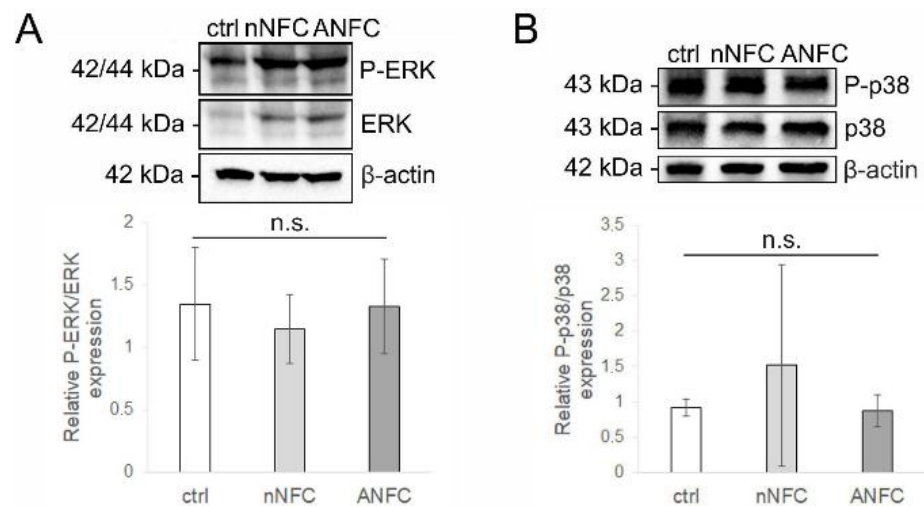


**Figure 8.** Extracellular signal-regulated kinase (ERK) and p38 mitogen-activated protein kinase (MAPK) signaling in control and nanofibrillar cellulose (NFC) hydrogel-treated wounds on day 7. (A) Western blot and quantitation showing the phosphorylation of ERK, presented as the mean  $\pm$  SD ( $n = 3-4$ ). ERK phosphorylation is not affected by NFC hydrogels. (B) Western blot and quantitation presenting unchanged phosphorylation level of p38 MAPK by NFC hydrogels. The data represent the mean  $\pm$  SD ( $n = 3-4$ ). Ctrl, control; ANFC, anionic NFC; nNFC, native NFC; n.s., not significant.

#### 4. Discussion

The biomaterial properties including biocompatibility, water-retaining ability, mechanical and chemical properties, and scaffold structure affect its successful application in tissue engineering [44]. We decided to test different hydrogel concentrations of native (1.5%) and anionic NFC (3.2%) to give insight of the material behavior for different further applications of NFC hydrogel. The chemical nature of the two hydrogels is different, and therefore they show varying stiffness even in the same concentration. The 1.5 *w/w*% NFC hydrogel is a readily available commercial product. It would be promising to test its potential in treatment of humanized deep wounds and for possible use, e.g., as a cell delivery scaffold in the future. ANFC hydrogel is a more novel form of NFC in the field of pharmaceutical applications, and it has an advantage of being transparent and easily moldable, which makes it an interesting biomaterial. In this study, we aimed to perform the preliminary *in vivo* tests with 3.2 *w/w*% ANFC hydrogel, which has previously shown potential in drug release [29]. We first addressed the morphology and water retention capacity of NFC hydrogels. Both native NFC and ANFC hydrogel showed a porous structure that may provide a sufficient space for the proliferation and migration of endogenous cells to facilitate tissue renewal. Regarding the swelling ratios, we observed that both NFC hydrogels show only a minor swelling behavior but long water-retaining capacity and no degradation during a period of 21 days. A proper moisture content is important for optimal wound healing, and therefore, both NFC hydrogels seem suitable for wound healing treatment due to their high water-retaining capacity. Further, our *in vitro* hemolysis assay revealed the non-hemolytic and thus biocompatible nature of both NFC hydrogels.

Repair of full-thickness wounds is initiated by the formation of granulation tissue that provides a platform for the new epithelial covering [45,46]. In humans, re-epithelialization

is the primary mechanism of wound healing accounting for up to 80% of wound closure [47]. Previously, it has been shown in a porcine full-thickness wound model that 1.7 *w/w%* native and 0.7 *w/w%* anionic NFC hydrogel both inhibit wound contraction and re-epithelialization with simultaneous increase in  $\alpha$ -SMA expression in the wound [24]. We have demonstrated here that native 1.5 *w/w%* native NFC hydrogel and 3.2 *w/w%* ANFC hydrogel do not significantly affect wound closure in the mouse splinted wound model. Further, neither native or anionic NFC hydrogel did impact granulation tissue formation or collagen deposition in wounds.

The re-epithelialization progressed through the proliferation of epidermal keratinocytes, which was not significantly influenced by NFC or ANFC hydrogel. Further, treatment with both NFC hydrogels showed similar growth of neo-epithelium compared with control. We have previously shown in a clinical study that a wound dressing manufactured from native NFC provides efficient wound epithelialization in skin graft donor site wounds [22,23], which is consistent with the results in the present study, which for the first time evaluates the performance of native NFC hydrogel in a humanized deep wound. During the entire healing process, continuous physical contraction appears in order to close the wound. After wounding, fibroblasts at the wound margins are activated by physical tension to differentiate into stress fiber-expressing proto-myofibroblasts [45]. Subsequently, these cells are activated by TGF- $\beta$ 1 secreted by inflammatory cells to  $\alpha$ -SMA expressing myofibroblasts, which have a key role in wound contraction [48]. We detected normal expression of  $\alpha$ -SMA, which proposed that contractile action of myofibroblasts is not affected by NFC or ANFC hydrogel.

Sufficient mechanical tension in a tissue is required for TGF- $\beta$ 1 activation and subsequent tissue maturation [34]. Our rheology measurement results indicate that both 1.5% NFC hydrogel and 3.2% ANFC hydrogel show elastic behavior due to having higher elastic modulus compared with loss modulus [49]. However, we discovered that ANFC hydrogel possesses higher elastic modulus compared with native NFC, but the different stiffness did not show differential effects on wound healing. The results suggest that both NFC hydrogels provide an optimal mechanical signal for tissue regeneration. Furthermore, the stiffness of NFC and ANFC hydrogel is able to be modified as a function of water content for different applications and according to the tissue in question.

In light of optimal wound healing, a correct balance in skin repair, i.e., time of wound closure, is important to enable optimal tissue regeneration but to avoid excess scarring. Therefore, we addressed the level of fibrosis after treatment with native NFC and ANFC hydrogels by comparing the expression levels of fibrotic markers TGF- $\beta$ 1 and collagen I to control and concluded that either of NFC hydrogels do not induce excess scarring. These results are in line with our previous study, where we showed that NFC wound dressing manufactured from native NFC and used for patient skin graft donor site treatment did not form a scar after epithelialization [23].

Application of a biomaterial often initiates recruitment of immune cells that are critical for regeneration and wound healing after injury [33,50–52]. In our study, we found that both native and anionic NFC hydrogel provoke a normal inflammatory response that is required for successful wound healing. Moreover, we observed infiltration of different cell types into the hydrogels but no foreign body response, which is characterized by multinucleated foreign body giant cells that form via macrophage fusion and that adhere on the biomaterial surface [53]. These results suggest an interactive connection to take place between the hydrogels and the tissue. Previously, anionic NFC scaffold has been shown to provoke a foreign body response when implanted subcutaneously due to slow degradation in a tissue over time [54]. However, this will not be an issue when NFC is applied topically. Recently, the importance of an interface between biomaterial and tissue has been recognized to enable cell adhesion, infiltration, and proliferation, which guides stimulation of tissue regeneration [55]. From tissue engineering perspective, it is important that the host tissue is able to successfully integrate and remodel the biomaterial into a functional substitute tissue.

Angiogenesis is a prerequisite for tissue regeneration since blood vessels provide the necessary nutrients and oxygen supply for the tissue. We analyzed the presence of CD31-positive blood vessels in the wound area and showed that NFC or ANFC hydrogel do not impede angiogenesis. With respect to signaling pathways underlying wound healing, we analyzed ERK and p38 MAPK signaling in wounds and showed that their phosphorylation is not affected by either of NFC hydrogels.

In clinical use of commercial hydrogels, they are often treated with saline for their removal from the wound bed. We observed dehydration of both hydrogels during the treatment. Therefore, in future applications it may be worthwhile to hydrate the hydrogels during the treatment to improve the outcome of wound healing.

Previously, surface chemistry has been shown to play a role in different biological responses towards biomaterials, including nanofibrillar cellulose [56]. In our study, we did not observe different behavior with respect to wound healing between native and anionic NFC hydrogel. Since both NFC and ANFC hydrogel is applicable as a cell scaffold for 3D cell culturing [19,28,57,58], they serve as potential scaffold materials for therapeutic cells to be used for wound treatment to stimulate wound healing. Additionally, they may provide a scaffold for delivery of drugs or proteins into a wound [19,29]. In summary, both NFC hydrogels may have potential clinical significance in postoperative wound management in the future and they may serve as a therapy for different types of wounds although native NFC hydrogel seems more promising based on the received results. However, this study presents only preliminary findings, and it is important to uncover the cellular and molecular processes that regulate wound healing before development of new therapies to modulate wound healing.

The limitations of the study include the small sample and animal number resulting from exclusion criteria, mainly because of splint failures, and that the wound healing was not evaluated until complete wound closure due to the same reason. The results are, however, promising and show the biocompatibility and mechanical characteristics of native and anionic NFC hydrogels, and a primary proof of concept of the application of NFC hydrogels in wound healing. A further study should be systematically designed and performed to validate the potential of NFC hydrogels as wound dressing using more animals.

In summary, native NFC hydrogel and ANFC hydrogel were shown to provide comparable wound closure rate and re-epithelialization compared with control. Wound healing in NFC and ANFC hydrogel-treated wounds progressed with normal inflammation, granulation tissue formation, and angiogenesis, and showed equal number of myofibroblasts, and level of fibrosis compared with control treatment.

## 5. Conclusions

In the present study, we found that native and anionic NFC hydrogels are biocompatible and facilitate wound closure and re-epithelialization comparable to control. Wounds treated with NFC and ANFC hydrogels progress through normal inflammatory reaction, re-epithelialization, granulation tissue formation, vascularization, and fibrotic remodeling. Future studies with NFC hydrogels may prove their potential as biomaterial scaffolds to be used to stimulate wound healing via delivery of a therapeutic agent to the wound.

**Supplementary Materials:** The following are available online at <https://www.mdpi.com/article/10.3390/micro1020015/s1>. Supplementary Materials and Methods: Power analysis and Randomization; Supplementary Table S1: Originally planned treatment groups; Supplementary Figure S1: In vivo wound treatments; Supplementary Table S2: The number of valid samples used for analyses; Supplementary Figure S2: Randomization of animals used for surgery.

**Author Contributions:** Conceptualization, R.K., K.L., M.N. and M.Y.; methodology, Q.X.; validation, R.K.; formal analysis, R.K.; investigation, R.K., Q.X., J.S., I.L.-S. and A.M.; resources, K.L., M.N., W.W. and M.Y.; data curation, R.K.; writing—original draft preparation, R.K. and J.S.; writing—review and editing, Q.X., I.L.-S., A.M., K.L., M.N., W.W. and M.Y.; visualization, R.K.; supervision, W.W. and M.Y.; project administration, R.K.; funding acquisition, R.K. and M.Y. All authors have read and agreed to the published version of the manuscript.

**Funding:** R.K. was funded by Osk. Huttunen Foundation, Finland. J.S. was supported by Doctoral Programme in Materials Research and Nanosciences (University of Helsinki, Finland). A.M. and M.Y. are thankful for the UPM GD-96 project. R.K. and M.Y. acknowledge the Business Finland and UPM-Kymmene funded Nanoskin projects.

**Institutional Review Board Statement:** The study was conducted according to the guidelines of the EU Directive 2010/63/EU and approved by the Animal Research Ethics Committee of University College Dublin (AREC-15-27-Wang, 22 November 2017), and by Health Products Regulatory Authority (AE18982/P091, 2 January 2018), Ireland.

**Informed Consent Statement:** Not applicable.

**Data Availability Statement:** The data presented in this study are available on request to the corresponding author.

**Acknowledgments:** We acknowledge UPM Biomedicals within UPM-Kymmene Corporation, Finland, for providing NFC materials for this study. HiLIFE Histotechnology, Laboratory Animal Pathology, and Histoscanner core facility (University of Helsinki) are acknowledged for providing support with histological techniques. SEM imaging was performed at the Helsinki Electron Microscopy Unit and fluorescence imaging at the Light Microscopy Unit (University of Helsinki) supported by Biocenter Finland. We are grateful to Leena Pietilä for helpful technical assistance.

**Conflicts of Interest:** K.L. and M.N. represent UPM-Kymmene Corporation, which is the manufacturer of NFC hydrogels. Other authors do not have conflicts of interest associated with this publication.

## Abbreviations

$\alpha$ -SMA	Alpha-smooth muscle actin
ANFC	Anionic nanofibrillar cellulose
BSA	Bovine serum albumin
CD31	Platelet endothelial cell adhesion molecule (PECAM-1)
Ctrl	Control
ECM	Extracellular matrix
ERK	Extracellular signal-regulated kinase
G'	Storage modulus
G''	Loss modulus
H&E	Hematoxylin and eosin
IHC	Immunohistochemical
MAPK	Mitogen-activated protein kinase
NFC	Nanofibrillar cellulose
nNFC	Native nanofibrillar cellulose
PBS	Phosphate-buffered saline
PCNA	Proliferating cell nuclear antigen
RBC	Red blood cell
RT	Room temperature
SD	Standard deviation
SEM	Scanning electron microscopy
TBS-T	Tris buffered saline with Tween 20
TEMPO	2,2,6,6-tetramethylpiperidine-1-oxyl
TGF- $\beta$ 1	Transforming growth factor beta 1

## References

1. Velnar, T.; Bailey, T.; Smrkolj, V. The Wound Healing Process: An Overview of the Cellular and Molecular Mechanisms. *J. Int. Med. Res.* **2009**, *37*, 1528–1542. [[CrossRef](#)]
2. Demidova-Rice, T.N.; Hamblin, M.R.; Herman, I.M. Acute and Impaired Wound Healing: Pathophysiology and current methods for drug delivery, part 1: Normal and chronic wounds: Biology, causes, and approaches to care. *Adv. Ski. Wound Care* **2012**, *25*, 304–314. [[CrossRef](#)]
3. Hoque, J.; Prakash, R.G.; Paramanandham, K.; Shome, B.R.; Haldar, J. Biocompatible Injectable Hydrogel with Potent Wound Healing and Antibacterial Properties. *Mol. Pharm.* **2017**, *14*, 1218–1230. [[CrossRef](#)]
4. Zhao, X.; Sun, X.; Yildirimer, L.; Lang, Q.; Lin, Z.Y.W.; Zheng, R.; Zhang, Y.; Cui, W.; Annabi, N.; Khademhosseini, A. Cell infiltrative hydrogel fibrous scaffolds for accelerated wound healing. *Acta Biomater.* **2017**, *49*, 66–77. [[CrossRef](#)]
5. Kong, X.; Fu, J.; Shao, K.; Wang, L.; Lan, X.; Shi, J. Biomimetic hydrogel for rapid and scar-free healing of skin wounds inspired by the healing process of oral mucosa. *Acta Biomater.* **2019**, *100*, 255–269. [[CrossRef](#)]
6. Kathawala, M.H.; Ng, W.L.; Liu, D.; Naing, M.W.; Yeong, W.Y.; Spiller, K.L.; Van Dyke, M.; Ng, K.W. Healing of Chronic Wounds: An Update of Recent Developments and Future Possibilities. *Tissue Eng. Part B Rev.* **2019**, *25*, 429–444. [[CrossRef](#)] [[PubMed](#)]
7. Chouhan, D.; Dey, N.; Bhardwaj, N.; Mandal, B.B. Emerging and innovative approaches for wound healing and skin regeneration: Current status and advances. *Biomaterials* **2019**, *216*, 119267. [[CrossRef](#)]
8. Soriano-Ruiz, J.L.; Gálvez-Martín, P.; Ruiz, E.L.; Suñer-Carbó, J.; Calpena-Campmany, A.C.; Marchal, J.A.; Clares-Naveros, B. Design and evaluation of mesenchymal stem cells seeded chitosan/glycosaminoglycans quaternary hydrogel scaffolds for wound healing applications. *Int. J. Pharm.* **2019**, *570*, 118632. [[CrossRef](#)] [[PubMed](#)]
9. Drury, J.L.; Mooney, D.J. Hydrogels for tissue engineering: Scaffold design variables and applications. *Biomaterials* **2003**, *24*, 4337–4351. [[CrossRef](#)]
10. Wang, C.; Varshney, R.R.; Wang, N.-A. Therapeutic cell delivery and fate control in hydrogels and hydrogel hybrids. *Adv. Drug Deliv. Rev.* **2010**, *62*, 699–710. [[CrossRef](#)]
11. Naahidi, S.; Jafari, M.; Logan, M.; Wang, Y.; Yuan, Y.; Bae, H.; Dixon, B.; Chen, P. Biocompatibility of hydrogel-based scaffolds for tissue engineering applications. *Biotechnol. Adv.* **2017**, *35*, 530–544. [[CrossRef](#)]
12. Kamoun, E.A.; Kenawy, E.-R.S.; Chen, X. A review on polymeric hydrogel membranes for wound dressing applications: PVA-based hydrogel dressings. *J. Adv. Res.* **2017**, *8*, 217–233. [[CrossRef](#)] [[PubMed](#)]
13. Bai, Q.; Han, K.; Dong, K.; Zheng, C.; Zhang, Y.; Long, Q.; Lu, T. Potential Applications of Nanomaterials and Technology for Diabetic Wound Healing. *Int. J. Nanomed.* **2020**, *15*, 9717–9743. [[CrossRef](#)]
14. Tavakoli, S.; Klar, A.S. Advanced Hydrogels as Wound Dressings. *Biomolecules* **2020**, *10*, 1169. [[CrossRef](#)] [[PubMed](#)]
15. Mantha, S.; Pillai, S.; Khayambashi, P.; Upadhyay, A.; Zhang, Y.; Tao, O.; Pham, H.M.; Tran, S.D. Smart Hydrogels in Tissue Engineering and Regenerative Medicine. *Materials* **2019**, *12*, 3323. [[CrossRef](#)]
16. Pourshahrestani, S.; Zeimaran, E.; Kadri, N.A.; Mutlu, N.; Boccaccini, A.R. Polymeric Hydrogel Systems as Emerging Biomaterial Platforms to Enable Hemostasis and Wound Healing. *Adv. Health Mater.* **2020**, *9*, 2000905. [[CrossRef](#)] [[PubMed](#)]
17. U.S. Food and Drug Administration (FDA). *Medical Devices Containing Materials Derived from Animal Sources (Except for In Vitro Diagnostics Devices) Guidance for Industry and Food and Drug Administration Staff*; U.S. Food and Drug Administration: Rockville, MD, USA, 25 March 2019; pp. 1–10.
18. Sahana, T.G.; Rekha, P.D. Biopolymers: Applications in wound healing and skin tissue engineering. *Mol. Biol. Rep.* **2018**, *45*, 2857–2867. [[CrossRef](#)]
19. Bhattacharya, M.; Malinen, M.M.; Laurén, P.; Lou, Y.-R.; Kuisma, S.W.; Kanninen, L.; Lille, M.; Corlu, A.; GuGuen-Guillouzo, C.; Ikkala, O.; et al. Nanofibrillar cellulose hydrogel promotes three-dimensional liver cell culture. *J. Control. Release* **2012**, *164*, 291–298. [[CrossRef](#)]
20. Junker, J.P.; Kamel, R.A.; Catterson, E.; Eriksson, E. Clinical Impact Upon Wound Healing and Inflammation in Moist, Wet, and Dry Environments. *Adv. Wound Care* **2013**, *2*, 348–356. [[CrossRef](#)]
21. Zhang, Y.; Nypelö, T.; Salas, C.; Arboleda, J.; Hoeger, I.C.; Rojas, O. Cellulose Nanofibrils. *J. Renew. Mater.* **2013**, *1*, 195–211. [[CrossRef](#)]
22. Hakkarainen, T.; Koivuniemi, R.; Kosonen, M.; Escobedo-Lucea, C.; Sanz-García, A.; Vuola, J.; Valtonen, J.; Tammela, P.; Mäkitie, A.; Luukko, K.; et al. Nanofibrillar cellulose wound dressing in skin graft donor site treatment. *J. Control. Release* **2016**, *244*, 292–301. [[CrossRef](#)]
23. Koivuniemi, R.; Hakkarainen, T.; Kiiskinen, J.; Kosonen, M.; Vuola, J.; Valtonen, J.; Luukko, K.; Kavola, H.; Yliperttula, M. Clinical Study of Nanofibrillar Cellulose Hydrogel Dressing for Skin Graft Donor Site Treatment. *Adv. Wound Care* **2020**, *9*, 199–210. [[CrossRef](#)]
24. Nuutila, K.; Laukkanen, A.; Lindford, A.; Juteau, S.; Nuopponen, M.; Vuola, J.; Kankuri, E. Inhibition of Skin Wound Contraction by Nanofibrillar Cellulose Hydrogel. *Plast. Reconstr. Surg.* **2018**, *141*, 357e–366e. [[CrossRef](#)] [[PubMed](#)]
25. Saito, T.; Kimura, S.; Nishiyama, Y.; Isogai, A. Cellulose Nanofibers Prepared by TEMPO-Mediated Oxidation of Native Cellulose. *Biomacromolecules* **2007**, *8*, 2485–2491. [[CrossRef](#)]
26. Alexandrescu, L.; Syverud, K.; Gatti, A.; Chinga-Carrasco, G. Cytotoxicity tests of cellulose nanofibril-based structures. *Cellulose* **2013**, *20*, 1765–1775. [[CrossRef](#)]

27. Azoidis, I.; Metcalfe, J.; Reynolds, J.; Keeton, S.; Hakki, S.S.; Sheard, J.; Widera, D. Three-dimensional cell culture of human mesenchymal stem cells in nanofibrillar cellulose hydrogels. *MRS Commun.* **2017**, *7*, 458–465. [[CrossRef](#)]
28. Sheard, J.J.; Bicer, M.; Meng, Y.; Frigo, A.; Aguilar, R.M.; Vallance, T.M.; Iandolo, D.; Widera, D. Optically Transparent Anionic Nanofibrillar Cellulose Is Cytocompatible with Human Adipose Tissue-Derived Stem Cells and Allows Simple Imaging in 3D. *Stem Cells Int.* **2019**, *2019*, 3106929. [[CrossRef](#)]
29. Paukkonen, H.; Kunnari, M.; Laurén, P.; Hakkarainen, T.; Auvinen, V.-V.; Oksanen, T.; Koivuniemi, R.; Yliperttula, M.; Laaksonen, T. Nanofibrillar cellulose hydrogels and reconstructed hydrogels as matrices for controlled drug release. *Int. J. Pharm.* **2017**, *532*, 269–280. [[CrossRef](#)] [[PubMed](#)]
30. Galiano, R.D.; Michaels, V.J.; Dobryansky, M.; Levine, J.P.; Gurtner, G.C. Quantitative and reproducible murine model of excisional wound healing. *Wound Repair Regen.* **2004**, *12*, 485–492. [[CrossRef](#)]
31. Dunn, L.; Prosser, H.C.G.; Tan, M.-J.; Vanags, L.Z.; Ng, M.K.C.; Bursill, C. Murine Model of Wound Healing. *J. Vis. Exp.* **2013**, *75*, e50265. [[CrossRef](#)]
32. Wright-Williams, S.; Flecknell, P.A.; Roughan, J.V. Comparative Effects of Vasectomy Surgery and Buprenorphine Treatment on Faecal Corticosterone Concentrations and Behaviour Assessed by Manual and Automated Analysis Methods in C57 and C3H Mice. *PLoS ONE* **2013**, *8*, e75948. [[CrossRef](#)] [[PubMed](#)]
33. Anderson, J.M.; Rodriguez, A.; Chang, D.T. Foreign Body Reaction to Biomaterials. In *Seminars in Immunology*; Elsevier: Amsterdam, The Netherlands, 2008; Volume 20, pp. 86–100.
34. Hinz, B.; Celetta, G.; Tomasek, J.J.; Gabbiani, G.; Chaponnier, C. Alpha-Smooth Muscle Actin Expression Upregulates Fibroblast Contractile Activity. *Mol. Biol. Cell* **2001**, *12*, 2730–2741. [[CrossRef](#)] [[PubMed](#)]
35. Ma, Z.; Shou, K.; Li, Z.; Jian, C.; Qi, B.; Yu, A. Negative pressure wound therapy promotes vessel destabilization and maturation at various stages of wound healing and thus influences wound prognosis. *Exp. Ther. Med.* **2016**, *11*, 1307–1317. [[CrossRef](#)] [[PubMed](#)]
36. Albelda, S.M.; A Muller, W.; A Buck, C.; Newman, P.J. Molecular and cellular properties of PECAM-1 (endoCAM/CD31): A novel vascular cell-cell adhesion molecule. *J. Cell Biol.* **1991**, *114*, 1059–1068. [[CrossRef](#)]
37. Horak, E.; Klenk, N.; Leek, R.; LeJeune, S.; Smith, K.; Stuart, N.; Harris, A.; Greenall, M.; Stepniewska, K. Angiogenesis, assessed by platelet/endothelial cell adhesion molecule antibodies, as indicator of node metastases and survival in breast cancer. *Lancet* **1992**, *340*, 1120–1124. [[CrossRef](#)]
38. Roberts, A.B.; Sporn, M.B.; Assoian, R.K.; Smith, J.M.; Roche, N.S.; Wakefield, L.; Heine, U.I.; Liotta, L.A.; Falanga, V.; Kehrl, J.H. Transforming growth factor type beta: Rapid induction of fibrosis and angiogenesis in vivo and stimulation of collagen formation in vitro. *Proc. Natl. Acad. Sci. USA* **1986**, *83*, 4167–4171. [[CrossRef](#)]
39. Desmoulière, A.; Geinoz, A.; Gabbiani, F. Transforming growth factor-beta 1 induces alpha-smooth muscle actin expression in granulation tissue myofibroblasts and in quiescent and growing cultured fibroblasts. *J. Cell Biol.* **1993**, *122*, 103–111. [[CrossRef](#)]
40. Border, W.A.; Noble, N.A. Transforming Growth Factor  $\beta$  in Tissue Fibrosis. *N. Engl. J. Med.* **1994**, *331*, 1286–1292. [[CrossRef](#)]
41. Loughlin, D.T.; Artlett, C.M. Modification of Collagen by 3-Deoxyglucosone Alters Wound Healing through Differential Regulation of p38 MAP Kinase. *PLoS ONE* **2011**, *6*, e18676. [[CrossRef](#)]
42. Escuin-Ordinas, H.; Li, S.; Xie, M.W.; Sun, L.; Hugo, W.; Huang, R.R.; Jiao, J.; De-Faria, F.M.; Realegeno, S.; Krystofinski, P.; et al. Cutaneous wound healing through paradoxical MAPK activation by BRAF inhibitors. *Nat. Commun.* **2016**, *7*, 12348. [[CrossRef](#)]
43. Beserra, F.P.; Xue, M.; Maia, G.L.D.A.; Rozza, A.L.; Pellizzon, C.H.; Jackson, C.J. Lupeol, a Pentacyclic Triterpene, Promotes Migration, Wound Closure, and Contractile Effect In Vitro: Possible Involvement of PI3K/Akt and p38/ERK/MAPK Pathways. *Molecules* **2018**, *23*, 2819. [[CrossRef](#)] [[PubMed](#)]
44. O'Brien, F.J. Biomaterials & scaffolds for tissue engineering. *Mater. Today* **2011**, *14*, 88–95. [[CrossRef](#)]
45. Rittié, L. Cellular mechanisms of skin repair in humans and other mammals. *J. Cell Commun. Signal.* **2016**, *10*, 103–120. [[CrossRef](#)]
46. Sorg, H.; Tilkorn, D.J.; Hager, S.; Hauser, J.; Mirastschijski, U. Skin Wound Healing: An Update on the Current Knowledge and Concepts. *Eur. Surg. Res.* **2017**, *58*, 81–94. [[CrossRef](#)] [[PubMed](#)]
47. Volk, S.W.; Bohling, M.W. Comparative wound healing: Are the small animal veterinarian's clinical patients an improved translational model for human wound healing research? *Wound Repair Regen.* **2013**, *21*, 372–381. [[CrossRef](#)] [[PubMed](#)]
48. Desmoulière, A.; Chaponnier, C.; Gabbiani, G. Tissue repair, contraction, and the myofibroblast. *Wound Repair Regen.* **2005**, *13*, 7–12. [[CrossRef](#)]
49. Pääkkö, M.; Ankerfors, M.; Kosonen, H.; Nykänen, A.; Ahola, S.; Österberg, M.; Ruokolainen, J.; Laine, J.; Larsson, P.T.; Ikkala, O.; et al. Enzymatic Hydrolysis Combined with Mechanical Shearing and High-Pressure Homogenization for Nanoscale Cellulose Fibrils and Strong Gels. *Biomacromolecules* **2007**, *8*, 1934–1941. [[CrossRef](#)]
50. Anderson, J.M. Inflammatory response to implants. *ASAIO Trans.* **1988**, *34*, 101–107. [[CrossRef](#)]
51. A DiPietro, L. Wound healing: The role of the macrophage and other immune cells. *Shock* **1995**, *4*, 233–240. [[CrossRef](#)]
52. Gurtner, G.C.; Werner, S.; Barrandon, Y.; Longaker, M.T. Wound repair and regeneration. *Nat. Cell Biol.* **2008**, *453*, 314–321. [[CrossRef](#)]
53. Sheikh, Z.; Brooks, P.J.; Barzilay, O.; Fine, N.; Glogauer, M. Macrophages, Foreign Body Giant Cells and Their Response to Implantable Biomaterials. *Materials* **2015**, *8*, 5671–5701. [[CrossRef](#)] [[PubMed](#)]
54. Rashad, A.; Suliman, S.; Mustafa, M.; Pedersen, T.Ø.; Campodoni, E.; Sandri, M.; Syverud, K.; Mustafa, K. Inflammatory responses and tissue reactions to wood-Based nanocellulose scaffolds. *Mater. Sci. Eng. C* **2019**, *97*, 208–221. [[CrossRef](#)] [[PubMed](#)]

- 
55. Sadtler, K.; Allen, B.W.; Estrellas, K.; Housseau, F.; Pardoll, D.M.; Elisseff, J.H. The scaffold immune microenvironment: Biomaterial-mediated immune polarization in traumatic and nontraumatic applications. *Tissue Eng. Part A* **2017**, *23*, 1044–1053. [[CrossRef](#)] [[PubMed](#)]
  56. Lopes, V.R.; Sanchez-Martinez, C.; Strømme, M.; Ferraz, N. In vitro biological responses to nanofibrillated cellulose by human dermal, lung and immune cells: Surface chemistry aspect. *Part. Fibre Toxicol.* **2017**, *14*, 1–13. [[CrossRef](#)] [[PubMed](#)]
  57. Lou, Y.-R.; Kanninen, L.; Kuisma, T.; Niklander, J.; Noon, L.A.; Burks, D.; Urtti, A.; Yliperttula, M. The Use of Nanofibrillar Cellulose Hydrogel As a Flexible Three-Dimensional Model to Culture Human Pluripotent Stem Cells. *Stem Cells Dev.* **2014**, *23*, 380–392. [[CrossRef](#)]
  58. Malinen, M.M.; Kanninen, L.; Corlu, A.; Isoniemi, H.M.; Lou, Y.-R.; Yliperttula, M.L.; Urtti, A.O. Differentiation of liver progenitor cell line to functional organotypic cultures in 3D nanofibrillar cellulose and hyaluronan-gelatin hydrogels. *Biomaterials* **2014**, *35*, 5110–5121. [[CrossRef](#)]